Science Journal of University of Zakho
DOI: https://doi.org/10.25271/sjuoz

Original Article

EFFECTS OF SEMI-INSULATING GALLIUM ARSENIDE SUBSTRATE ORIENTATIONS AND SPIN COATING SPEED ON THE ELECTRICAL PERFORMANCE OF PANI/SI-GAAS HYBRID PHOTODETECTOR DEVICES

Firas H. Ahmad [1], and Dler A. Jameel [2,*]

[1] Department of General Science, College of Basic Education, University of Zakho, Zakho, Kurdistan Region, Iraq.
[2] Department of Physics, College of Science, University of Zakho, Zakho, Kurdistan Region, Iraq.

[*]*Correspondence author, E-mail*: dler.jameel@.uoz.edu.krd (+964-7501881787)

Received:
06, Jul, 2025

Accepted:
10, Aug, 2025

Published:
12, Apr, 2026

ABSTRACT

This article presents the influence of semi-insulating gallium arsenide (SI-GaAs) orientations and spin coating speed (rotation per minute, rpm) on the electrical performance of hybrid organic/inorganic photodetector devices. Hybrid polyaniline (PANI)/SI-GaAs/Ag photodetector devices were fabricated by depositing PANI thin films on (111) A and (111)B SI-GaAs substrates at speeds of 2000 rpm and 3000 rpm using the spin coating technique. Device performance, evaluated through current–voltage (I–V) measurements under dark conditions and illumination with 532 nm light at varying power intensities, revealed a notable dependence on both substrate orientation and spin speed. The PANI/(111)B SI-GaAs at 2000 rpm devices revealed optimal performance at 0.58 mW.cm^{-2} with a photo response ratio of 3.16, responsivity (R) of 0.362 mA/W, detectivity (D*) of 2.05x10^{9} Jones, and external quantum efficiency (EQE%) of 8.44x10^{-2}. The PANI/(111)B SI-GaAs devices fabricated at spin rates of 2000 rpm exhibit a decreasing trend in all three photodetector performance parameters with increasing light power intensity, while the PANI/(111)B SI-GaAs at 3000 rpm device increases slightly with increasing intensity, except at 0.75 mW·cm^{-2}, where it decreases. In contrast, the (111)A-based devices exhibited a consistent performance increase with rising light intensity from 0.58 mW.cm^{-2} to 1.52 mW.cm^{-2} across both spin rates. This approach of integrating organic and inorganic materials opens opportunities for producing flexible, high-performance, low-cost photodetectors for various optoelectronic applications.

KEYWORD: PANI, SI-GaAs orientation, Photodetector device, spin coating deposition, external quantum efficiency.

1. INTRODUCTION

Semiconductor polymers have significant interest as materials with potential for the manufacture of optoelectronic devices (Yakuphanoglu *et al*., 2006). Materials that combine the mechanical and chemical properties of organic compounds with the electrical properties of semiconducting materials are known as organic semiconductors (Lu *et al*., 2018). The organic polymers refer to conducting polymers, such as polyacetylene, polyaniline (PANI), poly pyrrole, polythiophene, and poly (phenylene-vinylene), which have electrical, electronic, magnetic, and optical characteristics that are comparable to those of metals (El-Zohary *et al*., 2013; Hasan *et al*., 2025). Organic semiconductors are widely employed in technologies, including organic light-emitting diodes (OLEDs), thin-film transistors (Dey *et al*., 2015; Gao & Gao, 2010; Lu *et al*., 2018), solar cell (Dyer-Smith & Nelson, 2012), photo detectors, photoconductors (Kamalasanan, 2011), organic field effect transistors (OFETs) (Kunkel *et al*., 2021), health monitoring, biosensing (Liao *et al*., 2025), anti-corrosion coating, microwave absorption, chemical sensor (Beygisangchin *et al*., 2021), screen printing, and sensors (Majeed *et al*., 2022).

Polyaniline (PANI), originally known as black aniline, has several forms depending on its oxidation level. Moreover, PANI is renowned for its environmental stability, simplicity, and protonic acid doping capability (Beygisangchin *et al*., 2021). Furthermore, this conducting polymer is commonly utilized in electrochemical supercapacitors, functioning as a low-cost positive electrode material due to its excellent doping and de-doping characteristics and consistent oxidation state (Gazal *et al*., 2018; Khan *et al*., 2023). It is important to mention that in the PANI material, the majority of the charge carriers are holes which confirms that PANI is a p-type semiconductor (Jameel, 2021; Malhotra & Ali, 2018) PANI, a class of conjugated organic conductive electroactive polymers, exhibits electrical conductivity of up to 100 S/cm in ambient conditions, as does its emeraldine salt (L *et al*., 2018).

A semi-insulating GaAs crystal is characterized by high resistivity and a Fermi level near the mid-gap (Zanotti, 1983). The best choice for improving the design of monolithic X-ray and particle detectors is SI-GaAs. Semi-insulating gallium arsenide (SI-GaAs) single crystals are a significant material for the fabrication of integrated circuits (ICs) and microwave devices.

Access this article online
https://doi.org/10.25271/sjuoz.2026.14.2.1673

Printed ISSN 2663-628X;
Electronic ISSN 2663-6298

Science Journal of University of Zakho
Vol. 14, No. 02, pp. 309 –315 April-2026

SI-GaAs is characterized by low noise, high working temperature, high saturation velocity, and high electron mobility compared with silicon (Si) (Chen *et al*., 2000; Chen *et al*., 2002). At room temperature, semi-insulating GaAs exhibits a resistivity of $>10^7$ Ω cm and a broad band gap of 1.43 eV (Veale *et al*., 2014). However, the most common use for III–V compound semiconductors in recent years has been in the production of electrical and optoelectronic devices, specifically gallium arsenide (GaAs). High-index GaAs substrates, such as (311)B GaAs and (311)A GaAs, have attracted more attention nowadays (Jameel *et al*., 2016; Jameel *et al*., 2020; Mustafa *et al*., 2020). The incorporation of impurities and defects is significantly influenced by the substrate crystallographic orientation, and therefore, on the optical and electrical characteristics of devices (Al Huwayz *et al*., 2023; Shafi *et al*., 2010)

Koutsaroff *et al.* (2011) investigated the effects of semi-insulating GaAs crystal orientation on surface passivation efficacy. They discovered that various orientations (like (100), (110), and (111)) have an effect on passivation stability and density of surface states, which in turn affects device performance (Koutsaroff *et al*., 2011). Favennec (1976) studied the location, thickness, carrier concentration, and doping impurity of a semi-insulating layer that forms in GaAs using high-energy oxygen ions. He showed that deep double-electron traps are compensated for by small amounts of oxygen atoms (Favennec, 1976).

Photodetectors are essential parts of optoelectronic integrated circuits, which are utilized in biomedical imaging, optical communication systems, and connectivity. They provide high dynamic range, low noise, fast speed, and high sensitivity (El-Batawy *et al*., 2016) environmental monitoring and sensing (Gao *et al*., 2024).

The production of heterojunctions from two-dimensional (2D) materials has recently drawn considerable interest for a range of applications, for example, energy, optoelectronic devices, etc. (Watanabe *et al*., 2004). Recent studies demonstrate that metal nanostructures such as graphene can significantly enhance light–matter interactions in various 2D photodetectors (Rohizat *et al*., 2021), MoS2 (Abdullah Ripain *et al*., 2023), WS2 (Liu *et al*., 2019), MoTe2 (Chen *et al*., 2019), and many more. Liu *et al.* (2023) have described the process by which a photodetector for a CNAuF/TiO2 Schottky junction with a rise time of 110 ms and a decay time of 120 ms achieves an external quantum efficiency of 13.8%, a high specific detectivity of 3.9×10^9 Jones, and a responsivity of 0.06 A/W, respectively.

Although previous studies have investigated PANI-based photodetectors on silicon and GaAs substrates separately (Debnath *et al*., 2024; Shaker *et al*., 2024), no prior work has reported the fabrication and characterization of a PANI/SI-GaAs heterojunction photodetector. This article aims to study the PANI/SI-GaAs photodetector devices deposited on (111)A and (111)B orientations for the first time using spin-coating at 2000 and 3000 rpm. This research focuses on the intrinsic photo response of the PANI/SI-GaAs interface. The impacts of spin speed and crystallographic orientation on the photodetector performance were thoroughly examined at room temperature and wavelength 532 nm incident light. Our results exhibit that the (111)B at 2000 rpm-based devices display better performance when compared with (111)B at 3000 rpm, (111)A at 2000 rpm and (111)A at 3000 rpm devices.

2. EXPERIMENTAL DETAILS

In this research, SI-GaAs wafers with (111)A and (111)B orientations were used as inorganic substrates for PANI thin film deposition. Prior to deposition, the (111)A and (111)B substrates were cleaned using acetone and methanol, washed with deionized water, and dried with a nitrogen gas spray. Subsequently, a backside Ohmic contact of silver (Ag) was deposited by the sputtering technique (Baptista *et al*., 2018; Pérez-Zenteno *et al*., 2025). Details of the PANI synthesis and polymer solution preparation technique have been reported by Felix *et al.* (2011). After the production of the backside contact, PANI thin films were deposited onto (111)A and (111)B SI-GaAs substrates using the spin-coating technique at speeds of 2000 and 3000 rpm.

Finally, circular electrical contacts of silver (Ag) with an area of 0.0615 cm^2 were made on top of the SI-GaAs substrate to create PANI/(111)A SI-GaAs/Ag and PANI/(111)B SI-GaAs/Ag heterojunction device structures. The current-voltage (I-V) measurements were carried out under both dark and illuminated (532 nm with different light intensities) conditions at room temperature using an I-V source meter (model Keithley 2450) as illustrated in Figure 1a. Figure 1b shows the structure of the PANI/SI-GaAs device with backside contact (Ag) and applied voltage across the structure. A green laser with a wavelength of 532 nm and a power of 500 mW has been used for illumination.

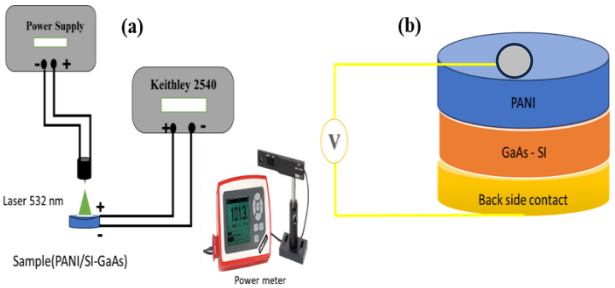

Figure 1: (a) Photodetector set-up for I-V measurements by Keithley 2450 and (b) Schematic diagram of PAN/SI-GaAs hybrid devices.

3. RESULTS AND DISCUSSION.

To study the impact of crystallographic orientation of SI-GaAs substrates and spin coating speed (rpm) on the photodetector performance of hybrid organic/inorganic photodetector devices, the current-voltage (I-V) measurements were performed on the PANI samples deposited with 2000 rpm and 3000 rpm on (111)A and (111)B SI-GaAs substrates. The I-V characteristics were conducted at room temperature in darkness (0 $mW.cm^{-2}$) and under incident light ranging from 0.58 $mW.cm^{-2}$ to 1.52 $mW.cm^{-2}$, corresponding to the calibrated power intensities over an effective area of 0.0615 cm^2, which aligns with the diameter of the laser beam. Measurements were conducted under a source-meter bias ranging from -5 V to +5 V.

Figure 2(a–d) displays that all samples demonstrated a rising trend in photocurrent as the light power intensity increased from 0.58 $mW.cm^{-2}$ to 1.52 $mW.cm^{-2}$. This suggests that higher light intensity increases photo-induced carrier generation due to enhanced photon absorption (Ismail *et al*., 2025). The photo response ratio is defined as the ratio of the photocurrent under 0.58 $mW.cm^{-2}$ illumination (red line in the graph) to the photocurrent in the dark (black line) for all samples. The PANI sample grown on (111)A SI-GaAs at 2000 rpm (Figure 2a) demonstrates a photo response ratio of 2.35. In contrast, the PANI sample deposited on (111)A SI-GaAs at 3000 rpm (Figure 2b) presents a ratio of 1.89. While the PANI sample grown on (111)B SI-GaAs at 2000 rpm (Figure 2c) reaches the highest ratio of 3.16, whereas for the same sample but at 3000 rpm (Figure 2d) records a ratio of 2.78. These results reveal that the (111)B at 2000 rpm sample has the highest photo-induced carrier generation under illumination, indicating superior sensitivity at low light intensities as compared with the (111)B at 3000 rpm, (111)A at 2000 rpm, and (111)A at 3000 rpm. These performance differences could be caused by variations in film thickness, making it an important focus for future research. The I-V characteristics under dark (see Figure 2e) of test samples consisting of only Ag/PANI/Ag/Glass presented Ohmic behavior in the examined reverse and forward voltage ranges. This result reveals that Ag forms an Ohmic contact with PANI

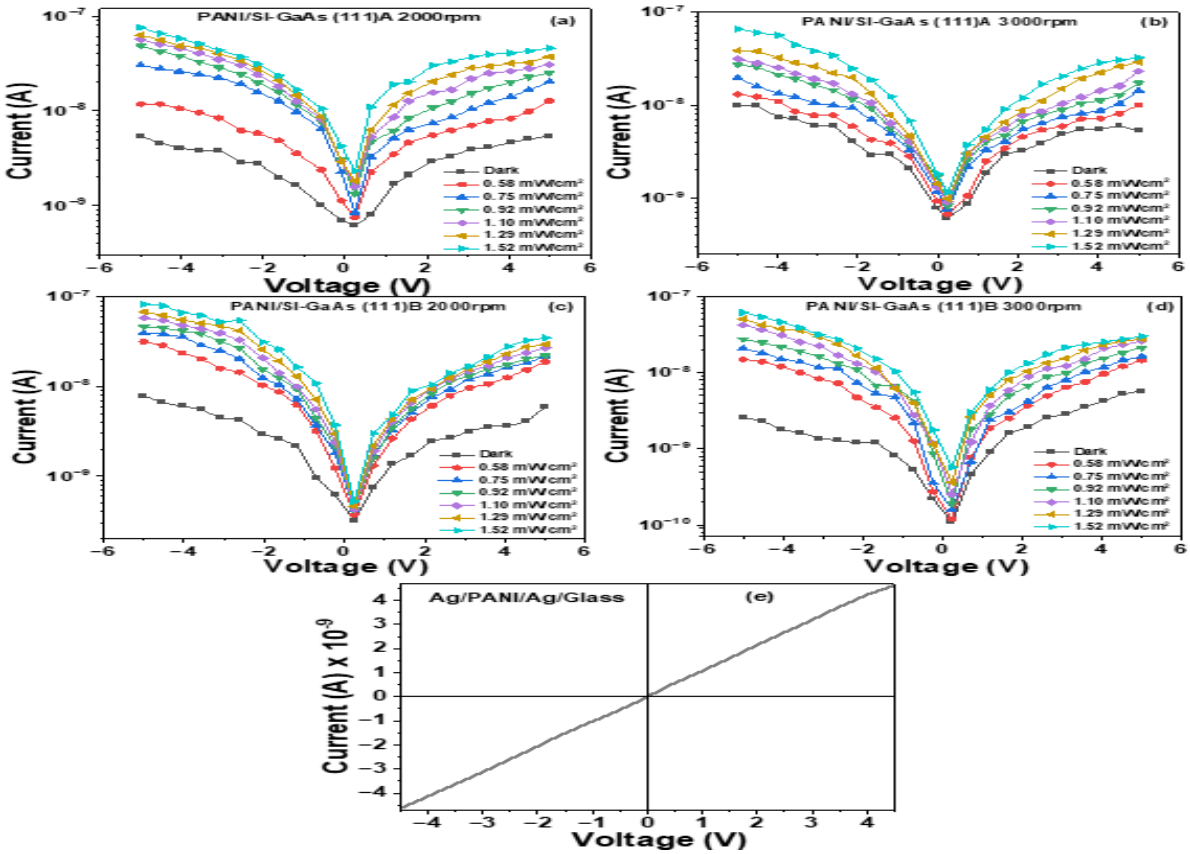

Figure 2: I-V curve in the dark and under 532 nm irradiation with varying intensity from 0.58 to 1.52 mW.cm^{-2} of (a) PANI/(111)A SI-GaAs/Ag at 2000 rpm, (b) PANI/(111)A SI-GaAs/Ag at 3000 rpm, (c) PANI/(111)B SI-GaAs/Ag at 2000 rpm, (d) PANI/(111)B SI-GaAs/Ag at 3000 rpm photodetector devices, and (e) Displays the Ohmic behavior between silver contact and PANI.

The photocurrent, $Photocurrent(I_{ph}) = I_{light} - I_{dark}$ where I_d is the dark current, I_{light} is the current under illumination, and I_{ph} is the photocurrent and is calculated by subtracting the dark current from the illuminated current. From Figure 3, the photocurrent of all samples increases with increasing power intensity. As a result, with an increase in photon energy, the device's photo-induced carrier concentration rises. Furthermore, it is revealed that the photocurrent at 0.58 mW.cm^{-2} and 0.75 mW.cm^{-2} for PANI/(111)B SI-GaAs at 2000 rpm is higher than that of other devices. Although the PANI/(111)B SI-GaAs device at 2000 rpm showed superior photocurrent at lower intensities, the (111)A counterpart outperformed at higher intensities (0.92–1.52 mW·cm^{-2}). In general, the devices for (111)B and (111)A at 2000 rpm are better than the (111)A and (111)B at 3000 rpm devices. These obtained performance variations are hypothesized to be due to changes in the thickness of the thin films.

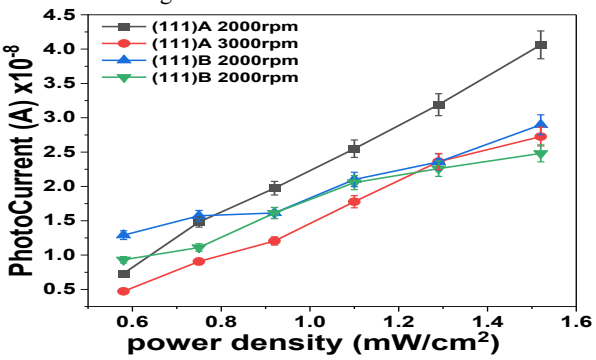

Figure 3: The photocurrent of (111)A and (111)B at 2000 and 3000 rpm devices versus the light power intensity.

The responsivity, $R = I_{ph}/(P_{int} \times A)$, is defined as the ratio of photocurrent produced by a device per unit area to the incident power intensity, calculated using I_{ph} for photocurrent, P_{int} for light power intensities (mW.cm^{-2}), and A for the active area of 0.0615 cm². The decrease in responsivity in the PANI/(111)B SI-GaAs at 2000 rpm device at larger light power intensities is primarily attributed to electron-trap saturation and an increase in electron-hole recombination (Ismail *et al*., 2023; Ismail *et al*., 2025). As more electrons enter the traps and produce more free electrons, the quasi-Fermi level energy rises. This result exhibits that the PANI/(111)B SI-GaAs at 2000 rpm device generates more photocurrent than the incident photons when exposed to reduced intensity of light (Ismail *et al*., 2025).

Figure 4a illustrates the responsivity of all samples. For the incident light of 0.58 mW.cm^{-2}, the PANI/(111)B SI-GaAs at 2000 rpm device shows higher responsivity of 0.362 mA/W compared to PANI/(111)B SI-GaAs at 3000 rpm, PANI/(111)A SI-GaAs at 2000 rpm and 3000 rpm devices that display responsivity of 0.262 mA/W, 0.21mA/W and 0.132 mA/W, respectively, at the bias voltage of + 5 V. The responsivity of the PANI/(111)B SI-GaAs at the 2000 rpm device decreases when the light power intensity increases. In contrast, the PANI/(111)A SI-GaAs at 2000 rpm and 3000 rpm devices demonstrate an increasing responsivity trend as the light intensity rises from 0.58 mW.cm^{-2} to 1.52 mW.cm^{-2}. This suggests that the PANI samples coated on (111)B devices are more responsive at lower light power density at 0.58 mW.cm^{-2}, making them more effective for low-intensity light response compared to the PANI samples coated on (111)A SI-GaAs with 2000 rpm and 3000 rpm speed coating. This value is lower than the responsivity (R) values reported by (Debnath *et al*., 2024) and (Li *et al*., 2024).

In addition to responsivity (R), detectivity (D^*) is another essential characteristic of device performance, defined as the device's capacity to detect a low signal, as described in Eq. (1) (Ismail *et al*., 2025).

$$D^* = \frac{R * \sqrt{A}}{\sqrt{2eI_d}} \text{ ---------- (1)}$$

Where A represents the active area (0.0615 cm^2), R is the responsivity, I_d indicates the dark current, and e is the electron charge. Figure 4b illustrates the detectivity behavior of all four devices. The PANI/(111)B SI-GaAs at 2000 rpm device exhibits a decreasing trend with increasing light power intensity. However, the PANI/(111)B at 3000 rpm device increases slightly with increasing intensity, whereas at 0.75 $mW.cm^{-2}$, it decreases. In contrast, the PANI/(111)A SI-GaAs devices at the same spin rates show an increasing detectivity trend as the light intensity rises from 0.58 $mW.cm^{-2}$ to 1.52 $mW.cm^{-2}$. This suggests that the (111)B devices are more sensitive at lower light power density (0.58 $mW.cm^{-2}$ making them more effective for low-intensity light detection compared to (111)A at 0.58 $mW.cm^{-2}$. It was observed that the D^* value of $2.05x10^9$ Jones obtained for (111)B at 2000 rpm device is higher than (111)B at 3000 rpm ($1.58x10^9$ Jones), (111)A at 2000 rpm ($1.22x10^9$ Jones), and (111)A at 3000 rpm ($7.99x10^8$ Jones) devices. It means that the PANI/(111)B SI-GaAs at 2000 rpm and 3000 rpm device is more capable of producing photocurrent at low light signals than the other two devices, owing to the optimal capacity of increasing light absorption in the SI-GaAs substrate, resulting in higher photocurrent.

To better understand the effect of orientation and spin coating speed on the photodetector performance, the external quantum efficiency (EQE (%)) is a measure related to device performance, defined as the amount of photocurrent created per light power using photon energy. The value of EQE can be derived through the following formula (Ismail *et al*., 2025):

$$EQE(\%) = \frac{hc}{e} \times \frac{R}{\lambda} \text{ ----------(2)}$$

Where c is the speed of light, h is Planck's constant, e is the electron charge, λ is the incident wavelength, and R is the responsivity. Figure 4c shows that EQE(%) decreases with optical power intensities ranging from 0.58 $mW.cm^{-2}$ to 1.52 $mW.cm^{-2}$ for PANI/(111)B SI-GaAs at a 2000 rpm device. Whilst for the PANI/(111)B at 3000 rpm device, there is a small increase in the value of EQE with increasing intensity, but at 0.75 $mW.cm^{-2}$ it decreases. However, the EQE(%) value of PANI/(111)A SI-GaAs at 2000 rpm and 3000 rpm devices increases as power intensity increases. At a power intensity of 0.58 $mW.cm^{-2}$, the EQE (%) for PANI/(111)B SI-GaAs 2000 rpm is calculated to be $8.44x10^{-2}$ which is larger than of $6.09x10^{-2}$, $4.79x10^{-2}$ and $3.09x10^{-2}$ for PANI grown on (111)B SI-GaAs at 3000 rpm, (111)A at 2000 rpm, and (111)A at 3000 rpm devices, respectively.

In general, at 0.58 $mW.cm^{-2}$, the larger EQE(%) obtained in PANI/SI-GaAs (111)B and (111)A at 2000 rpm is associated with absorbed photons expanding to more significant electron vibrations close to the surface of (111)A and (111)B at 3000 rpm for both devices, which affects recombination and carrier generation. Figure 4(a-c) shows that (111)A and (111)B at 2000 rpm devices perform better than (111)A and (111)B at 3000 rpm. This demonstrates more effective light trapping and carrier recombination inside (111)A and (111)B at 2000 rpm than (111)A and (111)B at 3000 rpm at this wavelength. In addition, the observed performance differences are believed to result from variations in film thickness, which will be a crucial focus of future research. The detectivity (D*) and external quantum efficiency EQE (%) values of the fabricated devices in this work are lower than those achieved by (Halge *et al*., 2024) and (Shaker *et al*., 2024). These could be related to defects or interface states acting as recombination or traps in the PANI/SI-GaAs devices.

Table 1 summarizes the figure of merit (FOM) of each device, with PANI/(111)B SI-GaAs at 2000 rpm having the greatest responsivity of 0.362 mA/W, detectivity of $2.05x10^9$ Jones, and a higher EQE(%) of 8.44 $x10^{-2}$ than all three devices. The PANI/(111)A SI-GaAs at 3000 rpm has the lowest FOM, with a responsivity of 0.132 mAW^{-1}, a lower detectivity of $7.99x10^8$ Jones, and a lower EQE(%) of 3.09 $x10^{-2}$.

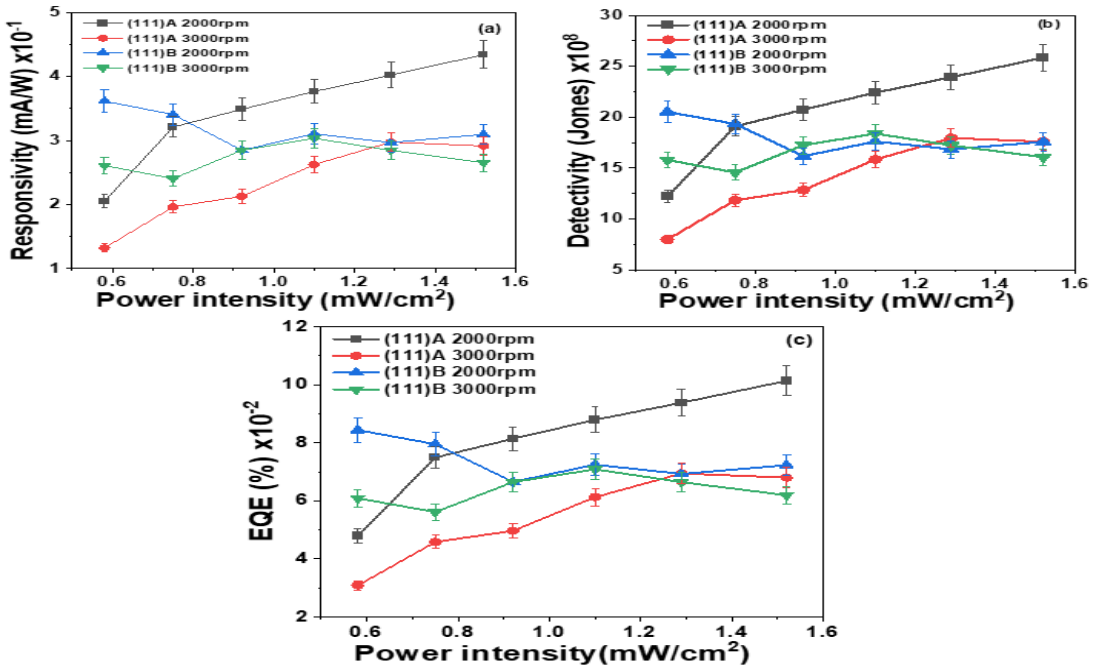

Figure 4: Figure of merit for (a) responsivity, (b) detectivity, and (c) EQE (%) for all photodetector samples.

Table 1. Overview of the figures of merit for all samples under illumination with 532 nm light at an intensity power of 0.58 mW.cm^{-2}.

Devices	Responsivity (mA/W)	Detectivity (Jones)	EQE (%)
(111)B 2000	0.362	2.05x 10^{9}	8.44 x 10^{-2}
(111)B 3000	0.261	1.58 x 10^{9}	6.09 x10^{-2}
(111)A 2000	0.205	1.22 x 10^{9}	4.79 x 10^{-2}
(111)A 3000	0.132	7.99 x 10^{8}	3.09 x10^{-2}

CONCLUSION

In conclusion, this article presented a novel strategy to enhance photodetector performance through integrating a PANI/SI-GaAs heterostructure device, where GaAs substrates with (111)A and (111)B orientations are used, and a thin film of PANI is coated with different spin-coating speeds (rotations per minute, rpm). The photodetector parameters of the PANI/SI-GaAs hybrid devices have been investigated by I-V measurements under visible light (532 nm) at different light intensities varying from 0.58mW/cm^2 to 1.52 mW.cm^{-2}. From the I-V characteristics, the optimized device displays a responsivity of 0.361 mA/W, a specific detectivity of 2.05×10^9 Jones, and a high photo response ratio of 3.16, and EQE (%)8.44 x10^{-2} with the best performance observed at 0.58 mW.cm^{-2} for the (111)B SI-GaAs device at 2000 rpm, outperforming all other configurations. Moreover, the responsivity, detectivity, and external quantum efficiency of the hybrid photodetector device (111)B at both rates were initially high; however, these parameters decreased with increasing light intensity for PANI/(111)B device at 2000 rpm, but for PANI/(111)B at 3000 rpm device increase slight with increase intensity, except at 0.75 mW.cm^{-2}, where it decreases. In contrast, the hybrid photodetector device (111)A at 2000 rpm and 3000 rpm reveals low responsivity, detectivity, and external quantum efficiency at low light intensity. Nevertheless, these values increase as the light intensity rises. This may be associated with variations in trap densities or differences in recombination mechanisms at the interfaces. This 2D organic semiconductor–semi–insulating–metal hybrid approach offers a promising route to developing cost-effective, high-performance photodetectors for future optoelectronic and sensing technologies.

Acknowledgements:

The author would like to thank the Centre for Materials Science and Nanotechnology, the Department of Physics, and the College of Science at the University of Zakho, Kurdistan Region, Iraq. Also, the authors wish to acknowledge Prof. Mohamed Henini from the University of Nottingham, UK, for his support and contributions.

Ethical approval:

This research does not require ethical approval because it is for educational purposes and does not involve human participants.

Author Contributions:

F. H. A: experimental design, writing, carrying out measurements, and manuscript composition; D. A. J: experimental design and manuscript composition.

Conflict of interest:

The authors declare that they have no known competing financial interests or personal relationships that could have appeared to influence the work reported in this paper.

Funding:

None.

REFERENCES

Abdullah Ripain, A., Zulkifli, N., Tan, C. L., W.H, A. M., & Zakaria, R. (2023). Highly efficient and stable near-infrared photo sensor based on multilayer MoS2/p-Si integrated with plasmonic gold nanoparticles. *Applied physics letters*, *123*. https://doi.org/10.1063/5.0158836

Al Huwayz, M., Jameel, D. A., Alotaibi, S., Alhassan, S., Almalki, A., Al Saqri, N., Al Saleh, Y., Alhassni, A., Almunyif, A., Lemine, O. M., Salhi, A., & Henini, M. (2023). Effects of substrate material on the electrical properties of self-assembled InAs quantum dots-based laser structures. *Applied Physics A*, *129*(6), 405. https://doi.org/10.1007/s00339-023-06626-w

Baptista, A., Silva, F., Porteiro, J., Míguez, J., & Pinto, G. (2018). Sputtering Physical Vapour Deposition (PVD) Coatings: A Critical Review on Process Improvement and Market Trend Demands. *Coatings*, *8*(11), 402. https://www.mdpi.com/2079-6412/8/11/402

Beygisangchin, M., Abdul Rashid, S., Shafie, S., Sadrolhosseini, A. R., & Lim, H. N. (2021). Preparations, Properties, and Applications of Polyaniline and Polyaniline Thin Films-A Review. *Polymers (Basel)*, *13*(12). https://doi.org/10.3390/polym13122003

Chen, N., Zhong, X., Lin, L., Xie, X., & Zhang, M. (2000). Semi-insulating GaAs grown in outer space. *Materials Science and Engineering: B*, *75*(2), 134-138. https://doi.org/https://doi.org/10.1016/S0921-5107(00)00348-2

Chen, N. F., Zhong, X. R., Zhang, M., & Lin, L. Y. (2002). Space grown semi-insulating gallium arsenide single crystal and its application. *Advances in Space Research*, *29*(4), 537-540. https://doi.org/https://doi.org/10.1016/S0273-1177(01)00662-7

Chen, W., Liang, R., Liu, Y., Zhang, S., Cheng, W., Zhao, L., & Xu, J. (2019). Surface plasmon-enhanced photodetection in MoTe2 phototransistors with Au nanoparticles. *Applied physics letters*, *115*(14). https://doi.org/10.1063/1.5116644

Debnath, S., Meyyappan, M., & Giri, P. K. (2024). Printed MoSe2/GaAs Photodetector Enabling Ultrafast and Broadband Photodetection up to 1.5 μm. *ACS*

Applied Materials & Interfaces, *16*(7), 9039-9050. https://doi.org/10.1021/acsami.3c17477

Dey, A., Singh, A., Das, D., & Iyer, P. (2015). Organic Semiconductors: A New Future of Nanodevices and Applications. 97-128. https://doi.org/10.1007/978-3-319-14774-1_4

Dyer-Smith, C., & Nelson, J. (2012). Chapter IE-2 - Organic Solar Cells. In A. McEvoy, T. Markvart, & L. Castañer (Eds.), *Practical Handbook of Photovoltaics (Second Edition)* (pp. 543-569). Academic Press. https://doi.org/https://doi.org/10.1016/B978-0-12-385934-1.00016-7

El-Batawy, Y., Mohammedy, F. M., & Deen, M. J. (2016). 13 - Resonant cavity enhanced photodetectors: Theory, design and modeling. In B. Nabet (Ed.), *Photodetectors* (pp. 415-470). Woodhead Publishing. https://doi.org/https://doi.org/10.1016/B978-1-78242-445-1.00013-0

El-Zohary, S. E., Shenashen, M. A., Allam, N. K., Okamoto, T., & Haraguchi, M. (2013). Electrical Characterization of Nanopolyaniline/Porous Silicon Heterojunction at High Temperatures. *Journal of Nanomaterials*, *2013*(1), 568175. https://doi.org/https://doi.org/10.1155/2013/568175

Favennec, P. N. (1976). Semi-insulating layers of GaAs by oxygen implantation. *Journal of Applied Physics*, *47*(6), 2532-2536. https://doi.org/10.1063/1.322970

Felix, J. F., de Vasconcelos, E. A., da Silva, E. F., & de Azevedo, W. M. (2011). Fabrication and electrical characterization of polyaniline/silicon carbide heterojunctions. *Journal of Physics D: Applied Physics*, *44*(20), 205101. https://doi.org/10.1088/0022-3727/44/20/205101

Gao, H. J., & Gao, L. (2010). Scanning tunneling microscopy of functional nanostructures on solid surfaces: Manipulation, self-assembly, and applications. *Progress in Surface Science*, *85*(1), 28-91. https://doi.org/https://doi.org/10.1016/j.progsurf.2009.10.001

Gao, L., Kang, B., Wu, H., & Jiang, S. (2024). Low power photodetector based on graphene-WS2-Au structure. *AIP Advances*, *14*(4). https://doi.org/10.1063/5.0207447

Gazal, U., Khan, I., Usmani, M. A., & Bhat, A. H. (2018). 11 - Modification of polymer nanocomposites and significance of ionic liquid for supercapacitor application. In M. Jawaid & M. M. Khan (Eds.), *Polymer-based Nanocomposites for Energy and Environmental Applications* (pp. 315-332). Woodhead Publishing. https://doi.org/https://doi.org/10.1016/B978-0-08-102262-7.00011-8

Halge, D. I., Narwade, V. N., Kaawash, N. M. S., Khanzode, P. M., Shaikh, S. J., Dadge, J. W., Alegaonkar, P. S., Hyam, R. S., & Bogle, K. A. (2024). High-performance blue light photodetector based on PANI/CdS heterojunction. *Materials Science in Semiconductor Processing*, *171*, 108020. https://doi.org/https://doi.org/10.1016/j.mssp.2023.108020

Hasan, M. B., Parvez, M. M., Abir, A. Y., & Ahmad, M. F. (2025). A review on conducting organic polymers: Concepts, applications, and potential environmental benefits. *Heliyon*, *11*(3), e42375. https://doi.org/https://doi.org/10.1016/j.heliyon.2025.e42375

Ismail, M., Abdullah Ripain, A., Ahmad Fahri, M., Zulkifli, N., & Zakaria, R. (2023). Size-dependent of plasmonic gold nanoparticles enhanced on WS2/Si nanohybrids photodetector. *Journal of Materials Science: Materials in Electronics*, *34*. https://doi.org/10.1007/s10854-023-10582-9

Ismail, M. N. S. M., Fahri, M. A. S. A., Tan, C. L., & Zakaria, R. (2025). Plasmon-enhanced visible photodetectors based on hexagonal boron nitride (hBN) with gold (Au), silver (Ag), and non-alloyed bimetallic (Au/Ag) nanoparticles. *Scientific Reports*, *15*(1), 6. https://doi.org/10.1038/s41598-024-84337-9

Jameel, D. A. (2021). Electrical performance of organic/inorganic hybrid solar cell devices based on n-type GaAs substrate orientations and a conjugated polymer (PANI). *Applied Physics A*, *127*(7), 570. https://doi.org/10.1007/s00339-021-04718-z

Jameel, D. A., Aziz, M., Felix, J. F., Al Saqri, N., Taylor, D., Albalawi, H., Alghamdi, H., Al Mashary, F., & Henini, M. (2016). Electrical performance of conducting polymer (SPAN) grown on GaAs with different substrate orientations. *Applied Surface Science*, *387*, 228-236. https://doi.org/https://doi.org/10.1016/j.apsusc.2016.06.097

Jameel, D. A., Marroquin, J. F. R., Aziz, M., Al Saqri, N. A., Jum'h, I., Telfah, A., Henini, M., & Felix, J. F. (2020). Investigation of the effects of GaAs substrate orientations on the electrical properties of sulfonated polyaniline based heterostructures. *Applied Surface Science*, *504*, 144315. https://doi.org/https://doi.org/10.1016/j.apsusc.2019.144315

Kamalasanan, M. N. (2011). Organic Semiconductors and its Applications. *AIP Conference Proceedings*, *1391*(1), 23-26. https://doi.org/10.1063/1.3646770

Khan, J., Khan, A., Rubab, B., Jamshaid, F., Al-Kahtani, A. A., & Dahshan, A. (2023). Exploring the progression of energy storage toward flexibility: Metal-organic framework and conducting polymer aspects. *Applied Materials Today*, *34*, 101906. https://doi.org/https://doi.org/10.1016/j.apmt.2023.101906

Koutsaroff, I., Edirisinghe, C. H., Ruda, H., Jedral, L. Z., Liu, Q., Guo-Ping, J., Xia, H., Lennard, W., & Rodriguez-Fernandez, L. (2011). Orientation Dependence Of Surface Passivation For Semi-Insulating Gaas. *MRS Proceedings*, *421*. https://doi.org/10.1557/PROC-421-93

Kunkel, C., Margraf, J. T., Chen, K., Oberhofer, H., & Reuter, K. (2021). Active discovery of organic semiconductors. *Nature Communications*, *12*(1), 2422. https://doi.org/10.1038/s41467-021-22611-4

L, Y., Niranjana, M., S P, A., H, V., S, R., & Hundekal, D. (2018). Characterization, Electrical Conductivity and Electrochemical Performance of Polyaniline-LiClO 4 - CuO Nano Composite for Energy Storage Applications. *Polymer-Plastics Technology and Engineering*, *58*, 1-13. https://doi.org/10.1080/03602559.2018.1466175

Li, B., Wang, K., Zhao, N., Fu, Z., Wang, M., Xie, Z., & Li, J. (2024). A high-performance organic–inorganic self-powered broadband photodetector based on

PANI/Bi2O2S nanocomposites [10.1039/D4TC02520B]. *Journal of Materials Chemistry C*, *12*(44), 17986-17995. https://doi.org/10.1039/D4TC02520B

Liao, C., Xiong, Y., Fu, Y., Chen, X., & Occhipinti, L. G. (2025). Organic semiconductors based wearable bioelectronics. *Wearable Electronics*, *2*, 23-39. https://doi.org/https://doi.org/10.1016/j.wees.2024.12.003

Liu, B., Xu, X., Han, M., Cheng, H., Chen, J., Sun, X., Zhang, Q., Duan, X., & Hu, J. (2023). Schottky junction made from a nanoporous Au and TiO2 film for plasmonic photodetectors. *ACS Applied Nano Materials*, *6*(6), 4619-4625.

Liu, Y., Huang, W., Chen, W., Wang, X., Guo, J., Tian, H., Zhang, H., Wang, Y., Yu, B., Ren, T.-L., & Xu, J. (2019). Plasmon resonance enhanced WS2 photodetector with ultra-high sensitivity and stability. *Applied Surface Science*, *481*, 1127-1132. https://doi.org/https://doi.org/10.1016/j.apsusc.2019.03.179

Lu, N., Li, L., Geng, D., & Liu, M. (2018). A review for polaron dependent charge transport in organic semiconductor. *Organic Electronics*, *61*, 223-234.

Majeed, A. H., Mohammed, L. A., Hammoodi, O. G., Sehgal, S., Alheety, M. A., Saxena, K. K., Dadoosh, S. A., Mohammed, I. K., Jasim, M. M., & Salmaan, N. U. (2022). A Review on Polyaniline: Synthesis, Properties, Nanocomposites, and Electrochemical Applications. *International Journal of Polymer Science*, *2022*(1), 9047554. https://doi.org/https://doi.org/10.1155/2022/9047554

Malhotra, B. D., & Ali, M. A. (2018). Chapter 4 - Biopolymeric Nanostructures: Biosensors and Bioimaging. In B. D. Malhotra & M. A. Ali (Eds.), *Nanomaterials for Biosensors* (pp. 127-144). William Andrew Publishing. https://doi.org/https://doi.org/10.1016/B978-0-323-44923-6.00004-2

Mustafa, H. A., Jameel, D. A., Salim, H. I., & Ahmed, S. M. (2020). The Effects Of N-GaAs Substrate Orientations on The Electrical Performance of PANI/N-GaAs Hybrid Solar Cell Devices. *Science Journal of University of Zakho*, *8*(4), 149-153. https://doi.org/10.25271/sjuoz.2020.8.4.773

Pérez-Zenteno, F., García-Hemme, E., Torres, I., Barrio, R., Duarte, S., Benítez-Fernández, R., Caudevilla, D., García-Hernansanz, R., Olea, J., Pastor, D., Prado, A. d., & San Andrés, E. (2025). High-pressure sputtering deposition and in situ plasma oxidation of TiOx thin films as electron selective contact for photovoltaic applications. *Materials Science in Semiconductor Processing*, *186*, 109038. https://doi.org/https://doi.org/10.1016/j.mssp.2024.109038

Rohizat, N. S., Ripain, A. H. A., Lim, C. S., Tan, C. L., & Zakaria, R. (2021). Plasmon-enhanced reduced graphene oxide photodetector with monometallic of Au and Ag nanoparticles at VIS–NIR region. *Scientific Reports*, *11*(1), 19688. https://doi.org/10.1038/s41598-021-99189-w

Shafi, M., Mari, R. H., Khatab, A., Taylor, D., & Henini, M. (2010). Deep-level Transient Spectroscopy of GaAs/AlGaAs Multi-Quantum Wells Grown on (100) and (311)B GaAs Substrates. *Nanoscale Research Letters*, *5*(12), 1948. https://doi.org/10.1007/s11671-010-9820-x

Shaker, S. S., Abdalsalam, A. H., & Ismail, R. A. (2024). Fabrication and characterization of polyaniline/Si heterojunction photodetector prepared by laser ablation in liquid. *Journal of Optics*. https://doi.org/10.1007/s12596-024-02160-x

Veale, M. C., Bell, S. J., Duarte, D. D., French, M. J., Schneider, A., Seller, P., Wilson, M. D., Lozinskaya, A. D., Novikov, V. A., Tolbanov, O. P., Tyazhev, A., & Zarubin, A. N. (2014). Chromium compensated gallium arsenide detectors for X-ray and γ-ray spectroscopic imaging. *Nuclear Instruments and Methods in Physics Research Section A: Accelerators, Spectrometers, Detectors and Associated Equipment*, *752*, 6-14. https://doi.org/https://doi.org/10.1016/j.nima.2014.03.033

Watanabe, K., Taniguchi, T., & Kanda, H. (2004). Direct-bandgap properties and evidence for ultraviolet lasing of hexagonal boron nitride single crystal. *Nature Materials*, *3*(6), 404-409. https://doi.org/10.1038/nmat1134

Yakuphanoglu, F., Başaran, E., Senkal, B., & Sezer, E. (2006). Electrical and Optical Properties of an Organic Semiconductor Based on Polyaniline Prepared by Emulsion Polymerization and Fabrication of Ag/Polyaniline/n-Si Schottky Diode. *The journal of physical chemistry. B*, *110*, 16908-16913. https://doi.org/10.1021/jp060445v

Zanotti, L. (1983). Semi-insulating GaAs technology: Recent and future developments. *Materials Chemistry and Physics*, *9*(1), 19-28. https://doi.org/https://doi.org/10.1016/0254-0584(82)90005-0